Astronomy and Computing 47 (2024) 100828

Contents lists available at ScienceDirect

Astronomy and Computing

journal homepage: www.elsevier.com/locate/ascom

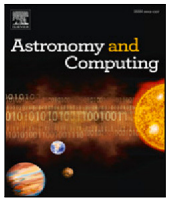

Full length article

# YOLO-ET: A Machine Learning model for detecting, localising and classifying anthropogenic contaminants and extraterrestrial microparticles optimised for mobile processing systems

L.J. Pinault [a,b,*], H. Yano [c,d], K. Okudaira [c,e], I.A. Crawford [a,b]

[a] School of Natural Sciences Birkbeck College, Malet Street, London, WC1E 7HX, United Kingdom
[b] Centre for Planetary Sciences at University College London/Birkbeck, Gower Street, London, 61E 6BT, United Kingdom
[c] The Institute of Space and Astronautical Sciences, Japan Aerospace Exploration Agency, 3-1-1 Yoshinodai, Chuo-ku, Sagamihara, Kanagawa, 252-5210, Japan
[d] Graduate University for Advanced Studies (SOKENDAI), 3-1-1 Yoshinodai, Chuo-ku, Sagamihara, Kanagawa, 252-5210, Japan
[e] Department of Computer Science and Engineering, University of Aizu, Aizu-Wakamatsu, Fukushima, 965-8580, Japan

ARTICLE INFO

Dataset link: http://github.com/apple/turicreate, https://github.com/LewisJPinault/YOLO-ET

*Keywords:*
Machine Learning
YOLO
Extraterrestrial materials
Lunar regolith
Aerogels
Anthropogenic contaminants

ABSTRACT

Imminent robotic and human activities on the Moon and other planetary bodies would benefit from advanced *in situ* Computer Vision and Machine Learning capabilities to identify and quantify microparticle terrestrial contaminants, lunar regolith disturbances, the flux of interplanetary dust particles, possible interstellar dust, $\beta$-meteoroids, and secondary impact ejecta. The YOLO-ET (ExtraTerrestrial) algorithm, an innovation in this field, fine-tunes Tiny-YOLO to specifically address these challenges. Designed for coreML model transference to mobile devices, the algorithm facilitates edge computing in space environment conditions. YOLO-ET is deployable as an app on an iPhone with LabCam® optical enhancement, ready for space application ruggedisation. Training on images from the Tanpopo aerogel panels returned from Japan's Kibo module of the International Space Station, YOLO-ET demonstrates a 90% detection rate for surface contaminant microparticles on the aerogels, and shows promising early results for detection of both microparticle contaminants on the Moon and for evaluating asteroid return samples. YOLO-ET's application to identifying spacecraft-derived microparticles in lunar regolith simulant samples and SEM images of asteroid Ryugu samples returned by Hayabusa2 and curated by JAXA's Institute of Space and Astronautical Sciences indicate strong model performance and transfer learning capabilities for future extraterrestrial applications.

## 1. Introduction

Extraterrestrial microparticles though millimetres or less in size, bear wide-ranging significance for understanding planetary system origins, delivery of water and life precursor materials to Earth and other planetary bodies, developing planetary protection measures, and identifying the distribution of potential resources in the Solar System. Missions to low Earth orbit, the Moon, asteroids and deep space destinations have already created a substantive inventory of these particles including:

1. Micrometeorites (MMs) — With their smaller mass, lower deceleration through the atmosphere and gentler Earth impact, some surviving micrometeorites are found to be relatively unaltered, with unmelted portions giving direct evidence of their precursor bodies and evolutionary sequence. MMs are generally categorised as meteoroids reaching the Earth's surface, and recovered like meteorites, with sizes in the 10s to 100s of μm (Dartois et al., 2013; Prasad et al., 2018; Rojas et al., 2021);
2. Interplanetary Dust Particles (IDPs) — Finer grained and captured in the stratosphere, with sizes up to 10 μm, IDPs are effectively a category of MMs, and are also presumed to be of asteroidal and cometary origin, like Antarctic Micrometeorites (AAMs) and Cosmic Spherules (CSs), fully melted and recondensated meteoroids recovered from the deepsea floor; (Flynn, 1994; Kurat et al., 1994);
3. Interstellar Dust Particles (ISPs) — Originating from outside our Solar system and owing to the Sun's Galactocentric orbit and other influences, these particles can travel at Earth encounter speeds of up to ~100 $\mathrm{km\,s^{-1}}$ or greater hypervelocities (Taylor et al., 1996);
4. Lunar and asteroidal regoliths — The Apollo and Luna missions of 1969–1976 and the Chang 'e 5 mission of 2020 returned dust

* Corresponding author at: School of Natural Sciences Birkbeck College, Malet Street, London, WC1E 7HX, United Kingdom.
*E-mail address:* l.pinault@ucl.ac.uk (L.J. Pinault).

https://doi.org/10.1016/j.ascom.2024.100828
Received 30 December 2023; Accepted 25 April 2024
Available online 3 May 2024

particles from the Moon to Earth, and the asteroid sample returns by Hayabusa in 2010 (Nakamura et al., 2011), Hayabusa2 in 2020 (Yada et al., 2022) and OSIRIS-REx in 2023 (Goldwin, 2023) also successfully added to Earth's inventory; and

5. Anthropogenic contaminants — Fragments from spacecraft exteriors, engines, spacesuit microfibres and outgassed materials from extravehicular activities are produced in both normal operations and as a result of material degradation and microparticle impacts in space. These are likely to accompany human and robotic activities on the Moon (e.g. Yano et al., 1994, 1997; Yamagishi et al., 2021).

Each of these categories of microparticles in and from the space environment has its own significance, but many are also interrelated, and in practice, on lunar and asteroid surfaces they may be mixed or amalgamated together. Micrometeorites may offer direct comparison to past asteroid and lunar sample returns for example, affording a recalibration of terrestrial micrometeorite collections by overcoming the selective biases of atmospheric entry, an important step toward better understanding Solar system formation processes (e.g. Genge et al., 2020).

Almost all microscopic analyses of extraterrestrial samples involve a detailed examination of their petrological features, textures, mineralogy, and chemical composition, drawing on a depth of research expertise, judgement and experience to offer classification suggestions and understand origins and implications for the early solar system and more. Besides a heavy experience requirement, the equipment required for these undertakings can be their own burden. Even the most recent automated micro-scanning systems in extraterrestrial sample labs, while increasingly powerful, are substantially sized and practically immobile (Sasaki et al., 2019). Their power-intensive requirements, slow speeds of operation and high consumption of computing resources can lead to lengthy processing times. Here we introduce a novel approach using Computer Vision and AI Machine Learning combined with advanced on-device optical and computing technologies, that can serve as an important complement to researchers' experience and a companion to their field efforts. These advancements can overcome the limitations of current systems to rapidly and accurately identify, localise, and classify microparticles making it a more robust and practical solution for *in situ* anthropogenic contaminant and extraterrestrial sample analyses.

In this study, we seek to harness the potential of AI Machine Learning to address a specific challenge in the planetary sciences: the identification and classification of micron to millimetre scale extraterrestrial particle impacts and features. The application of AI in image classification is a topic of fast-growing interest across various fields; our specific contributions are rooted in the novel application of these techniques to the unique domain of extraterrestrial particles, alongside the development of a specialised dataset and tailored training processes for their data handling.

We collect data from 'F (false)' samples which are not captured micrometeoroids but rather anthropogenic contaminants identified on the surfaces of the Tanpopo aerogel panels exposed outside of the JAXA Kibo module of the International Space Station. The data were prepared and imaged using a digital optical microscope, recording, and processing techniques designed for rapid and automated identification followed by initial morphological classification of the identified features by experienced space scientists (Section 2).

Following data acquisition and archiving, we introduce YOLO-ET (You Only Look Once ExtraTerrestrial), a modified YOLO deep learning algorithm trained on the aerogel panel images to provide an optimised pipeline for detecting these 'F' sample features (Section 3). We then analyse the performance of the trained model on unseen data in (Section 4.2) and conclude with discussions on the applications to anthropogenic contaminants introduced to lunar simulants, as well as micro-scaled features within asteroid Ryugu samples, and their potential correlations to micrometeorites from the TransAntarctic Mountains in (Section 6.1) and (Section 6.2) respectively.

## 2. Data acquisition and archiving

### 2.1. Astrobiology project Tanpopo

Tanpopo is Japan's first space experiment for astrobiology utilising the Exposure Facility of the Japan Experimental Module (JEM) of the International Space Station (ISS), designed for the exposure of extremophile microbes and astronomical organic analogues, and for the collection of potentially organic-bearing micrometeoroids impacting the ISS before entering the Earth's atmosphere, in order to explore the potential for and any evidence of two-way interplanetary transport of life precursors and life (Yamagishi et al., 2014). For impacting microparticles, including micrometeoroids, space debris, and possible terrestrial particles that might carry microbes as bioaerosols, the capture of these particles was achieved using silica aerogel capture panels (Tabata et al., 2011). These were first placed on the Exposed Experiment Handrail Attachment Mechanism (ExHAM) unit on the ISS in 2015–2019 for the Tanpopo mission and followed by the Tanpopo2 mission in 2019–2020 (Fig. 1).

The first set of silica aerogel panels was exposed for one year before being returned to Earth (Kawaguchi et al., 2016), and these aerogel panels were examined under the microscope in clean room facilities at the Institute of Space and Astronautical Sciences (ISAS) in Sagamihara Japan (Yamagishi et al., 2021). CLOXS, which stands for "Captured particles Locating Observation and eXtracting System" (Sasaki et al., 2019), is a specialised processing machine designed for the Tanpopo mission (Fig. 2). It processes the returned aerogel from space, placing them on an X-Y-Z coordinate stage, and autoscans and images them under the microscope to integrate a microscale map of the entire aerogel panel by moving the stage in micrometre increments (Fig. 3). When objects of interest are identified from the integrated mapping image by a scientist, the coordinates of the region of interest of the panel are recorded and the X-Y-Z stage can be automatically moved for revisiting the location for higher magnification investigation. The stack of the revisited images at different focal length depths may contain true penetration tracks and surface objects.

The Tanpopo mission's classification of surface impacts from hypervelocity impactors is pivotal to understanding not only the impact process, which can lead to vaporisation of the impactor, but also to glean information about the impactor's composition and origin from the remnants it leaves behind. Traditionally this involved laborious microscopic examination and imaging of 100s of samples, with inherent human errors, and earlier efforts by the authors focused on track types—carrot, pit crater, straight, and teardrop. The identified particles and particle impact tracks (Figs. 4 and 5) in the aerogel that are of interest are cut out into suitable-sized chips that contain impact tracks of particles captured in space, where a needle is then used to cut the aerogel without contamination; this is then distributed to research groups worldwide for detailed biological and chemical analyses of the captured microparticles (Yano et al., 2014).

As for microparticles collected on the surface of the Tanpopo aerogel panels, these are presumed not to be 'True' hypervelocity impactors associated with morphological features (i.e. carrot tracks, pit craters, straight tracks, and teardrop tracks), but rather 'False' incidentally collected particles impacted at much slower velocities such as material released by ISS docking and undocking activities, venting materials, secondary impacts from primary impact ejecta, possible spacecraft component fibres, and fragments of the aerogel itself. This study has prioritised accurately classifying surface residual effects of these 'F' samples, such as sputter, fibre, block, bar, and aerogel fragments. Semi-automated methods have been employed to enhance classification but until the work of this project, matching the expertise of human scientists has remained a challenge, requiring a series of manual resizings, whitening, and contrast adjustments to secure even modest levels of confidence. Given the abundance of samples, continuous improvement in automated techniques is essential to accurately assess the microparticle remnants.

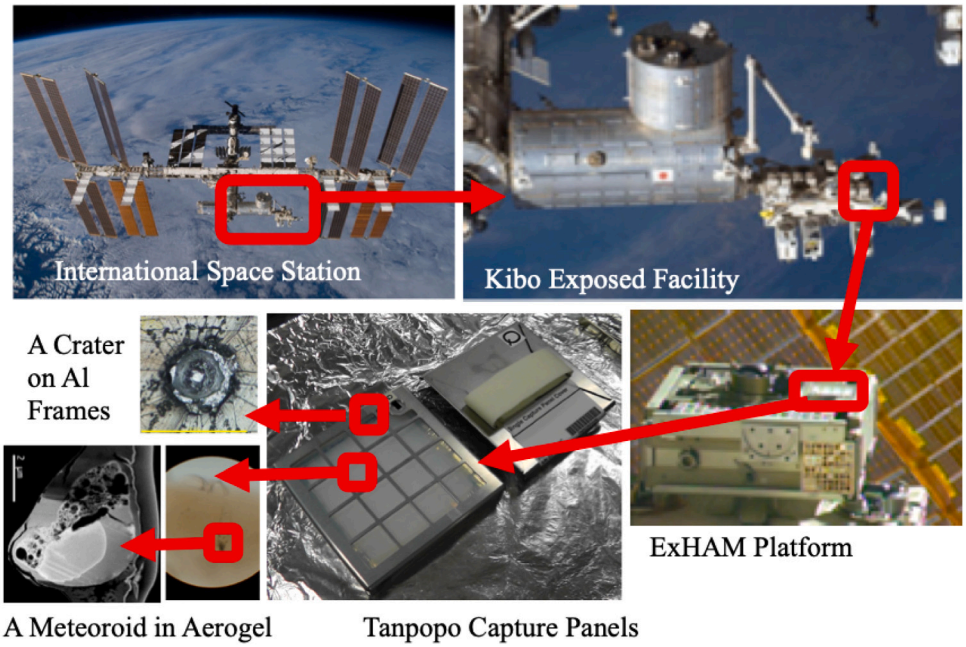


**Fig. 1.** Progressive zoom-in sequence of the Tanpopo astrobiology mission onboard the International Space Station (ISS), showing the placement of silica aerogel panels on the Kibo Exposed Facility for capturing impacting microparticles (Yamagishi et al., 2021). The sequence depicts the ISS with highlighted Kibo module, the ExHAM unit where aerogel panels are mounted, and close-up views of an impact crater on the aluminium frames of the panel and an aerogel panel in which an intact captured micrometeroid is discovered by subsequent analyses.

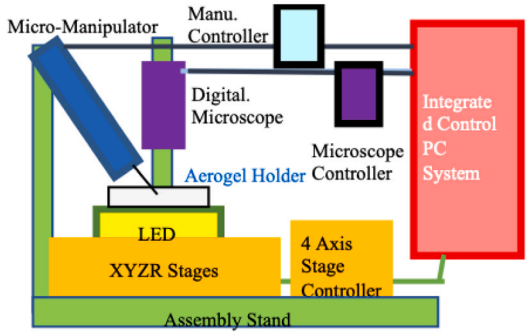


**Fig. 2.** Schematic representation of the CLOXS system, illustrating the precise arrangement of the micro-manipulator, aerogel holder, LED lighting, and XYZ stages mounted on an assembly stand, all coordinated by manipulator and microscope controllers, and integrated into a central control PC system for meticulous particle extraction and analysis.

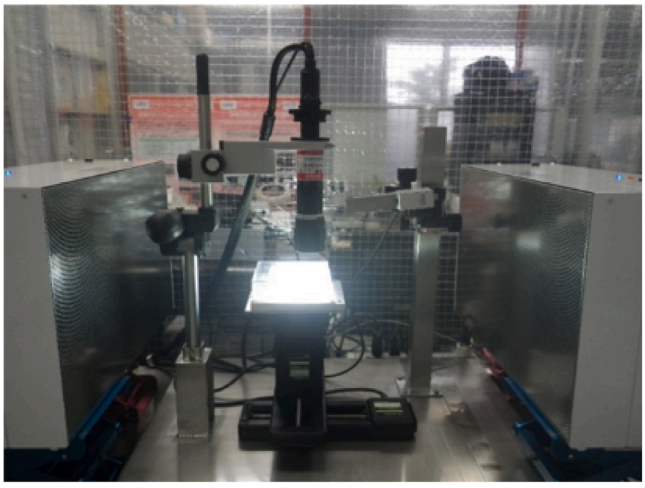

**Fig. 3.** The CLOXS system set-up in the ISAS clean room.

### 2.2. Machine learning dataset

This research focuses on the Tanpopo1-2 missions 2015–2020 collection of aerogel surface features larger than ~100 μm in the 10 cm × 10 cm aerogel panels captured at typically 100x to 245x magnifications. The total number of 'F' sample images in the collection is over 4000. In consideration for the computational power and memory limitations required to train machine learning models with large image input sizes, our data sample consists of 395 images, which is less than 10% of the total 'F' samples, in .jpeg format each 480 × 704 pixels in size. Our dataset is limited by the lack of annotated data (image-label pairs). With the open-source Python widget Bbox, we additionally manually annotate each image with a bounding box around each object (some images contain multiple particles and others none), and a class label of either 'sputter', 'block', 'fibre', 'bar', and 'aerogel fragment' (Fig. 6).

We note that the images have a variety of hues and brightnesses as they were captured under different lighting conditions, however in

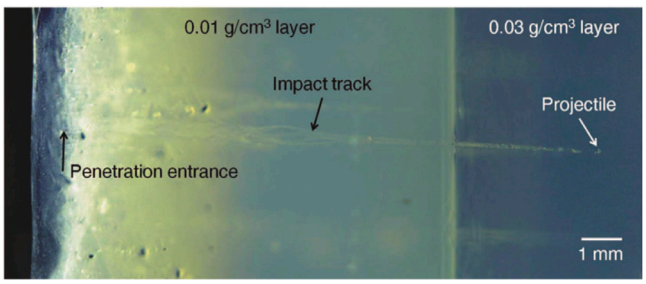


**Fig. 4.** Silica aerogel sample post-impact from a hypervelocity particle experiment, simulating the conditions for the Tanpopo project. This experiment conducted on Earth tests the resilience of the aerogel panels designed for microparticle collection onboard the ISS.
*Credit:* Tabata et al. (2011).

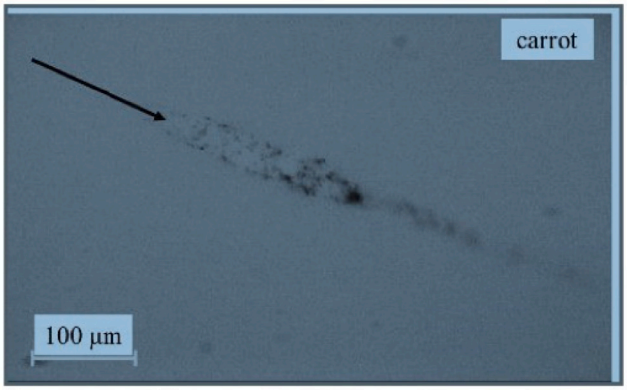


**Fig. 5.** A 'carrot' shaped track of a hypervelocity impactor in the Tanpopo silica aerogel panel returned from the International Space Station. The arrow indicates an impact direction.


**Fig. 6.** Examples of Tanpopo surface objects. From left to right, aerogel fragment, sputter, bar, block and fibre.

the interest of human time-saving we do not preprocess the images to account for this. Similarly we do not threshold, convert to grey scale or remove noise in the manner typically used to enhance the images for human inspection, as this would defeat the gains offered through the speed of Machine Learning. We are however inspired by the challenges and building on prior work using these more laborious methods (Krizhevsky, 2009; Krizhevsky et al., 2012).

We split our data sample into 80% for training (316 images) and 20% for testing (79 images). These are randomly sampled whilst maintaining the baseline ratio between different classes. The training data are the images used to optimise the model weights during the training phase of the model. The test data are not seen during the training of the model. We note that whilst it is common to additionally set aside a validation dataset for informing when the model is sufficiently trained — i.e. not under- or over- fit, our relatively limited data sample hampers our ability to reserve additional samples for validation, which could weaken the model's performance. Machine Learning methods are data greedy and perform better with more data, so to compensate for the relative data paucity, we apply automatic augmentation in the form of flipping the training images vertically, horizontally or both (corresponding to 180° rotation), resulting in a factor of 4 increase to the training sample (Fig. 7).

## 3. YOLO-ET: A highly efficient convolutional neural network for extraterrestrial microparticle detection and classification

### 3.1. Machine learning

Machine Learning (ML) (see Goodfellow et al., 2016, for a review) involves constructing layered architectures where each layer performs specific operations on data. These layers, particularly in neural networks, are composed of nodes or neurons with associated weights. During training, ML algorithms process input data through these layers, where each operation transforms the data based on the current weights.

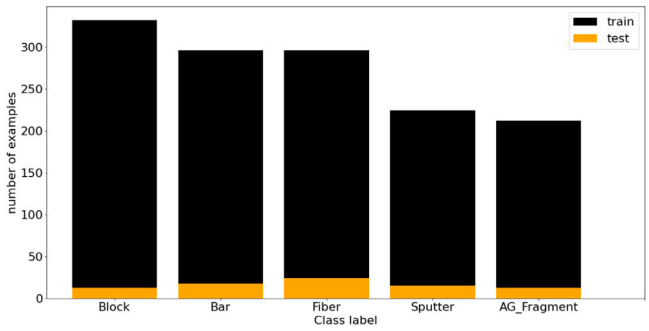


**Fig. 7.** Distribution of training and test data over the different classes. We note that these do not directly correspond to the number of images, as images can contain multiple objects of different classes or no objects altogether. Additionally there is significantly more training data as the augmentation is applied only to the training sample.

The goal is to optimise the weights to minimise a predefined cost or loss function (Section 3.3.2), which measures the difference between the algorithm's predictions and the actual outcomes. The optimisation is typically done using techniques like gradient descent, where the algorithm iteratively adjusts the weights based on the gradient of the loss, improving the model's predictions over time (Mitchell, 1997). Supervised learning, a subset of Machine Learning, involves algorithms that improve at tasks over time by learning from labelled data. Our project applies supervised learning to object detection, training models to recognise and categorise microscopic particles on aerogel panels. The data consists of pairs of images and their corresponding labels that are the bounding box coordinates (x and y), height (h), width (w), and class.

### 3.2. YOLO

Machine Learning (ML) algorithms employing Deep Learning techniques have been gaining traction in the astronomical sciences for nearly a decade, with applications ranging from galactic surveys (Huertas-Company and Lanusse, 2022), dark matter mapping (Jeffrey et al., 2020) and notably in regard to this work, galactic cluster detection (Grishin et al., 2023), using a streamlined YOLO technique. YOLO (Redmon et al., 2016), an acronym for "You Only Look Once", is a supervised learning approach to real-time object detection in computer vision. YOLO's novel architecture enables it to process images in a single pass, predicting both the bounding boxes and class probabilities (confidence scores) for objects within the image simultaneously. This contrasts with earlier two-step detection systems (e.g. Girshick, 2015), which would first propose regions and then classify them. The efficiency of YOLO allows it to detect objects rapidly with a high degree of accuracy, making it ideal for applications that require real-time processing.

Like more conventional techniques, YOLO is a type of convolutional neural network (CNN), consisting of a series of convolutional layers and pooling layers rather than neurons (Chen et al., 2021). Jaeger et al. (2021) use a 16-convolutional layer Visual Geometry Group CNN, VGG-16 (Simonyan and Zisserman, 2014) to classify impact craters on aluminium foils from the Stardust interstellar dust collector, which are typically less than one micrometre in size and sparse, making them difficult to find. While this method excels in accuracy for small objects, its deep architectures lacks YOLO's speed, limiting its use in real-time scenarios. Additionally, it primarily assesses the probability of crater presence without pinpointing exact locations, and is not optimised for images containing multiple objects of different classes.

### 3.3. YOLO-ET

YOLO-ET, is a modification of YOLO optimised for the detection of extraterrestrial microparticles. Specifically, we employ Tiny

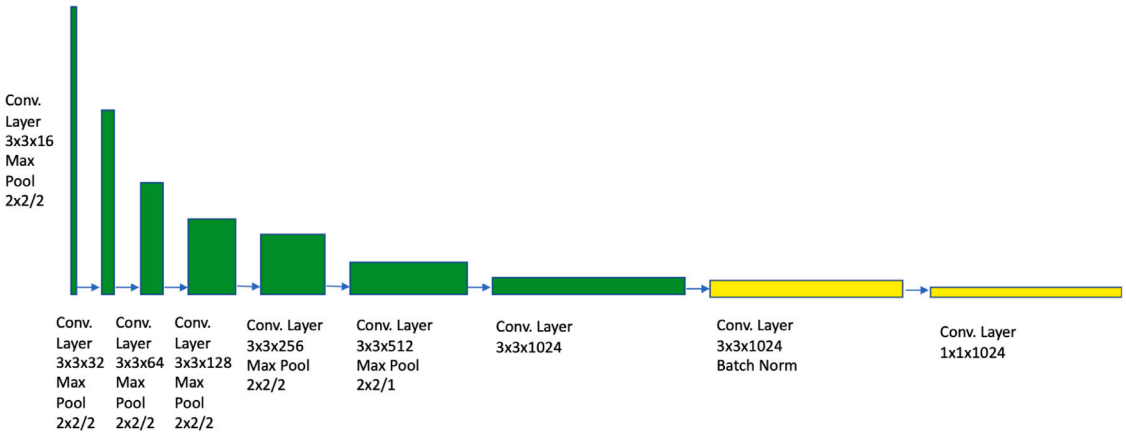


**Fig. 8.** TinyYOLOv2 architecture showing the series of convolutional and max pooling layers, with Batch Normalisation marked in yellow. The numbers represent the filter size and number of filters in each layer and the/represents the stride in the max pooling layers. Batch Normalisation is introduced after convolutional operations and before the activation functions, and leads to faster convergence during training by reducing internal covariate shift, i.e. the natural tendency to change the mean and variance of the inputs with each layer. Aside from helping to stabilise the training process by ensuring that the distribution of inputs to each layer remains more consistent during training, Batch Normalisation also helps regularise the model and reduce overfitting, so that the model can generalise better to unseen data.

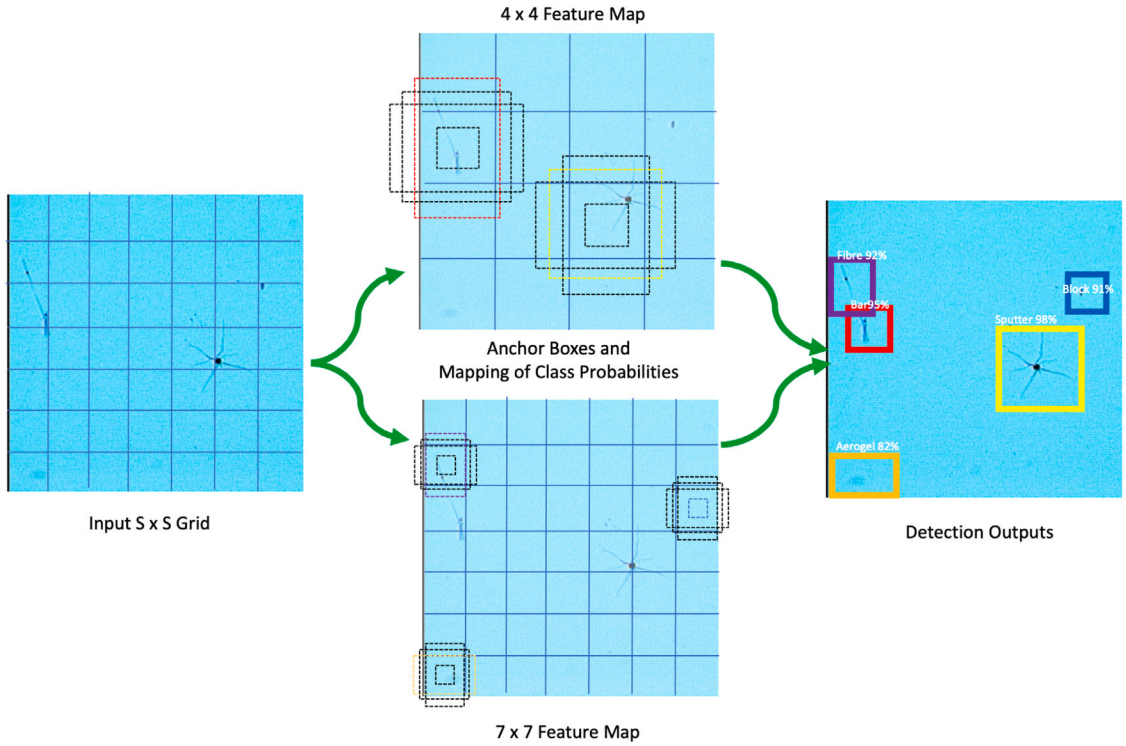


**Fig. 9.** Diagram illustrating the concept of anchor boxes in TinyYOLOv2, showcasing various predefined box shapes and sizes strategically positioned across a Tanpopo aerogel image in YOLO-ET implementation. These anchor boxes enable the efficient and accurate prediction of object boundaries and classifications within a single pass of the network.

YOLOv2 (Fig. 8), which is a smaller, simplified version of the original YOLOv2 (Redmon and Farhadi, 2017) with a Darknet-19 base network (a 19-layer network inspired by the VGG-16 model). For an overview on the development of YOLO see Jiang et al. (2022). YOLOv2 is designed to be more compact and faster than YOLO, making it suitable for applications with limited computational resources, such as mobile devices or real-time systems (see e.g. Zhou et al. (2022)). While maintaining the core principles of YOLO's single-pass detection, YOLOv2 simplifies the architecture with fewer convolutional layers and filters. In the original YOLO architecture, bounding box predictions were made relative to the dimensions of a grid cell; this approach had some limitations in terms of accuracy, particularly around predicting the correct size and location of objects. YOLOv2 improved upon this by predicting bounding box coordinates directly. Instead of the network learning offsets relative to a grid cell, YOLOv2 learns to predict bounding box coordinates relative to the location of the grid cell, along with anchor box dimensions, which makes predictions more precise (Fig. 9). This reduction in complexity results in faster processing speeds but typically at the cost of some detection accuracy compared to the full YOLO model. The "Tiny" version of YOLOv2 is specifically optimised to be more lightweight and faster, sacrificing some accuracy for the sake of speed and smaller model size. This makes Tiny YOLOv2 particularly well-suited for deployment in environments with limited computational resources, such as mobile devices, embedded systems, or applications where real-time performance is crucial. We underscore the suitability of the TinyYOLOv2 architecture for mobile use, which represents a significant advancement in deploying deep learning models on devices without the need for high-powered computing resources. YOLO-ET

thus embraces Tiny YOLOv2's trade-off between speed and precision, optimised for scenarios where real-time performance is crucial. For a deeper understanding of the efficiency and effectiveness of the TinyYOLOv2 architecture in mobile environments, we direct readers to the comprehensive study detailed in Zhou et al. (2022). This study provides empirical evidence supporting our choice of architecture, demonstrating its superior performance in scenarios demanding high efficiency and reliability on mobile devices.

#### 3.3.1. Non-maximum suppression

Non-maximum Suppression (NMS) (Neubeck and Van Gool, 2006) is a post-processing technique commonly used in object detection algorithms and is a key feature in YOLO and YOLOv2, that ensures each detected object is only recognised once. When an object detection model predicts multiple bounding boxes for the same object, NMS helps in selecting the most probable bounding box and discarding the rest. It does this by comparing the overlap between two boxes (A and B) using a metric called Intersection Over Union (IOU),

$$IOU = \left| \frac{A \cap B}{A \cup B} \right|, \tag{1}$$

and retaining only the boxes below the defined IOU threshold, and above the defined confidence score threshold while suppressing the others. This reduces redundancy and increases both detection interpretability and accuracy. The default IOU threshold and confidence threshold in our work are 0.5 and 0.3, respectively, providing both a limited clutter of redundant bounding boxes and a practical level of accuracy for distinguishing microparticle types.

#### 3.3.2. Loss function

The loss function quantifies the difference between the values predicted by the model and the actual values in the training data. A key goal in Machine Learning is to find the set of parameters, the weights and biases in the context of convolutional neural networks, that can optimise toward actual values by iteratively moving toward the minimum value of the loss function. The slope or derivative of the loss function with respect to its parameters is defined as its gradient, and moves in the direction of the steepest increase of the function. Moving in the opposite direction of the gradient, the algorithm iteratively adjusts the parameters to reduce loss, referred to as the gradient's descent. The learning rate is a hyperparameter that determines the size of the steps taken toward the minimum — too large, and the algorithm might overshoot the minimum, too small, and it will converge very slowly, consuming additional computing resource. Batch sizes determine the amount of data used to calculate the gradient at each step.

The YOLO loss function specifically combines terms for bounding box prediction accuracy, object presence confidence, and class prediction, ensuring the model is well-tuned across all aspects of object detection. In contrast to Grishin et al. (2023)'s work on galaxy clusters, YOLO-ET retains the comprehensive YOLO loss function, exploiting the full power of YOLO to simultaneously tackle the presence of multiple objects of different classes in an image. This is also useful for aerogel-captured particles, where multiple particles may overlap or appear at different depths in the aerogel panel, and it is essential for real world observational tasks in the planetary sciences like searching for microparticles and tell-tale microcraters *in situ* on the surface of the Moon.

Our loss function is defined as follows,

$$\begin{aligned} L = {} & \lambda_{\text{coord}} \sum_{i=0}^{s^2} \sum_{j=0}^{B} \mathbb{1}_{ij}^{obj} [(x_i - \hat{x}_i)^2 + (y_i - \hat{y}_i)^2] \\ & + \lambda_{\text{coord}} \sum_{i=0}^{s^2} \sum_{j=0}^{B} \mathbb{1}_{ij}^{obj} [(\sqrt{w_i} - \sqrt{\hat{w}_i})^2 + (\sqrt{h_i} - \sqrt{\hat{h}_i})^2] \\ & + \sum_{i=0}^{s^2} \sum_{j=0}^{B} \mathbb{1}_{ij}^{obj} (C_i - \hat{C}_i)^2 \\ & + \lambda_{\text{noobj}} \sum_{i=0}^{s^2} \sum_{j=0}^{B} \mathbb{1}_{ij}^{noobj} (C_i - \hat{C}_i)^2 \\ & + \sum_{i=0}^{s^2} \mathbb{1}_{ij}^{obj} \sum_{c \in \text{classes}} (p_i(c) - \hat{p}_i(c))^2, \end{aligned} \tag{2}$$

where, the first two terms, weighted by $\lambda_{\text{coord}}$, penalise errors in the position $(x, y)$ and size $(w, h)$ of predicted bounding boxes compared to the ground truth. These are crucial for precise localisation. The third term penalise errors in object scores $C_i$, distinguishing between object presence and absence. The fourth term, scaled by $\lambda_{\text{noobj}}$, specifically penalise false detections and the final term assesses the classification error for each class $c$ across the objects detected, ensuring accurate class predictions (Redmon et al., 2016).

#### 3.3.3. Turi Create

We deploy YOLOv2 through Turi Create,[1] an open-source machine learning library developed by Apple. It provides a simplified approach to creating machine learning models, especially for developers interested in practical field application. Turi Create supports various types of models, including classifiers, recommender systems, and image classifiers, and is particularly known for its ease of use in creating models for iOS apps. The library is optimised for scalability and performance, enabling the development and deployment of models on both Macs and mobile iOS devices. Using Turi Create for object identification, localisation, and image classification is remarkably straightforward, allowing more user development time for focusing on the customisation of the learning model itself. AI Machine Learning is becoming increasingly accessible and user-friendly with applications such as Turi Create and Microsoft Lobe[2] providing highly accessible implementation of AI including in educational settings.[3]

This user-friendly entry point into object detection provides a streamlined experience, but at the cost of customisation depth. This abstraction means users are not able to fine-tune all model hyperparameters, i.e. the configuration settings of the network defined before training begins. In the case of YOLO-ET, these include: the learning rate — i.e. the magnitude by which the weights are updated during training, the anchor box dimensions, the NMS (confidence) threshold and the IOU threshold. It is also not trivial to employ a validation set directly within the framework. However, TuriCreate still affords some degree of control, allowing for the adjustment of hyperparameters such as batch size and maximum iterations, which can significantly influence model performance and training time.

During training, we experimented with various batch sizes. While larger batches demand more memory due to the increased number of images loaded simultaneously, they tend to smooth out the loss curve, leading to a more stable model. Conversely, smaller batches, although more memory-efficient, can result in a noisier gradient descent trajectory. High-resolution inputs restricted our batch capacity, thereby decelerating the training convergence. Nevertheless, larger batches expedited convergence toward the global minimum of the loss function. For this project, a batch size of 32 was identified as the most effective, balancing computational resource demands and learning stability.

In the training of our model, an epoch is defined as one complete pass through the entire dataset, whereas an iteration is one update of the model's weights, which occurs after processing a batch of samples. Recall our model uses 1264 training images with a batch size of 32, each epoch consists of 1264/32 = 39.5, approximately 40 iterations. Setting max_iterations to 2000 means the training process involved

[1] https://github.com/apple/turicreate.

[2] https://www.lobe.ai/.

[3] Lobe requires neither Machine Learning nor coding experience and should enable a wide range of user engagements. Currently however its templates are only set up for Image Classification tasks.

roughly 2000/40 = 50 epochs. After experimenting with various numbers of max_iterations, 2000 was found to be optimal, striking a balance between model performance and computational efficiency. This choice was partly influenced by Turi Create's constraints on validation set usage, which limited our ability to employ traditional validation techniques to fine-tune the number of iterations. Instead, we relied on trial and error in the creation of the model, along with runtime considerations, to determine the most effective training duration. Since our goal is automated on-device deployment for laboratory and *in situ* use in space environments, the trial-and-error component in the model creation phase to achieve this goal is a practical trade off: the balance of convenience with a good modicum of configurability makes Turi Create a practical tool for rapid development, while recognising the limitations for more advanced experimentation and nuanced model optimisation.

#### 3.3.4. Transfer learning

Our dataset is relatively modest in size even with augmentation, but in order to train machine learning models effectively requires extensive datasets and prolonged computational training times. Transfer learning e.g. Tan et al. (2018) offers a practical solution to this challenge by utilising a pre-trained model – a model initially trained on a specific task and dataset – and adapting it to a different, yet related, task or dataset. This approach can take two forms:

- Direct Application: If the new task closely aligns with the original training task, the pre-trained model may be used as-is, leveraging its existing knowledge.
- Modification and Retraining: More commonly, the latter layers of the network are modified and retrained, while the initial layer weights are kept fixed. This tailors the model more closely to the new task and data.

Such a method is advantageous as it significantly reduces the volume of training data required and shortens the training time compared to training a model from scratch. This efficiency stems from the model's ability to build upon the knowledge already acquired during its initial training phase.

For further refinement, fine-tuning comes into play. This process involves making minor adjustments to the model's weights, already pre-trained on a large dataset, to achieve a more precise adaptation to the new task. Turi Create's implementation of TinyYOLO executes this process in a user-friendly manner. Initially, the model is pre-trained on the standard ImageNet dataset (Fei-Fei et al., 2009), which comprises over 1 million images of 224 × 224 resolution, spanning 1000 classes. This foundational training equips the model with a broad understanding of various visual features. Subsequently, it undergoes fine-tuning to adapt to higher-resolution images, specifically to a resolution of 448. This pre-trained model is further refined using our specialised Tanpopo dataset to create YOLO-ET. Using a desktop AMRadeon Pro Vega 64X 16 GB GPU, training time takes 0.02, 0.17 and 0.37 s per iteration for batch sizes of 1, 32 and 64 respectively. The runtime for prediction on 79 test images takes 1.14 s, demonstrating the efficient and practical application of transfer learning and fine-tuning in customising models for specific tasks in planetary and astronomical sciences, and opening the door to tasks that could be readily implemented on-device in laboratory and spacecraft environments.

## 4. Evaluation and results

Fig. 10 illustrates the model's training loss over time. While it may seem tempting to continue training until the loss approaches zero, it is critical to halt the training process beforehand to avoid overfitting. Overfitting occurs when a model becomes excessively attuned to the training data, to the extent that it perfectly predicts the classes and localisations. Such hyper-specific learning compromises the model's ability to generalise and perform accurately on new, unseen data. Therefore, identifying the right moment to stop training is essential for maintaining the model's effectiveness on diverse datasets. Evaluating the model on the test set that the model has not encountered during training, serves as a proxy for real-world, unseen data and provides a more accurate measure of how well it will perform in the real world in comparison to the training set (Fig. 11). Fig. 12 shows an example of the model applied to test data. Note that the NMS/IOU thresholds have failed at removing the duplicate detection, as both boxes are above the

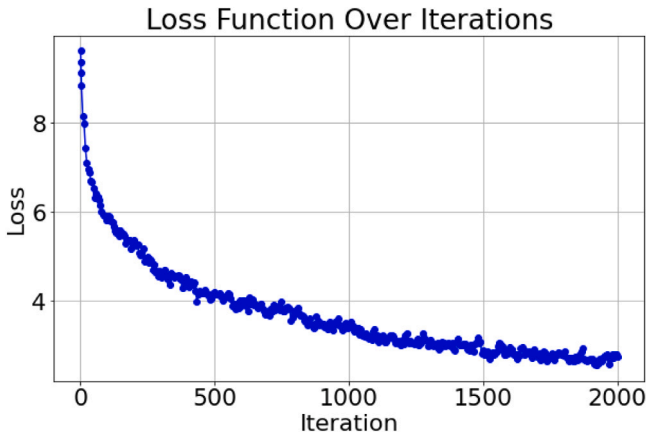


**Fig. 10.** YOLO-ET training loss of the network over time.

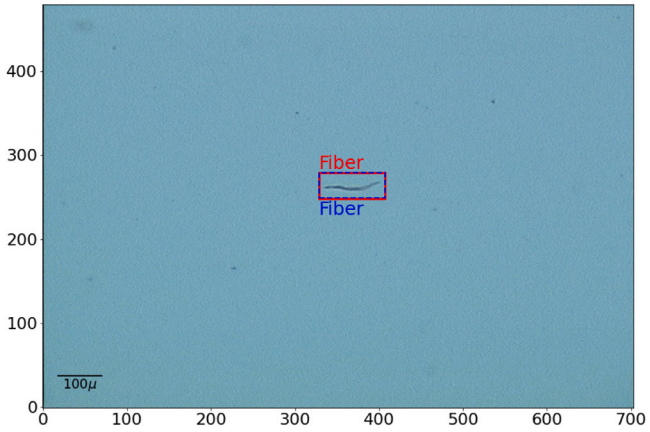


**Fig. 11.** Training example image depicting a fibre with the ground truth bounding box in dashed blue and the prediction from the network in red. Units are pixel coördinates.

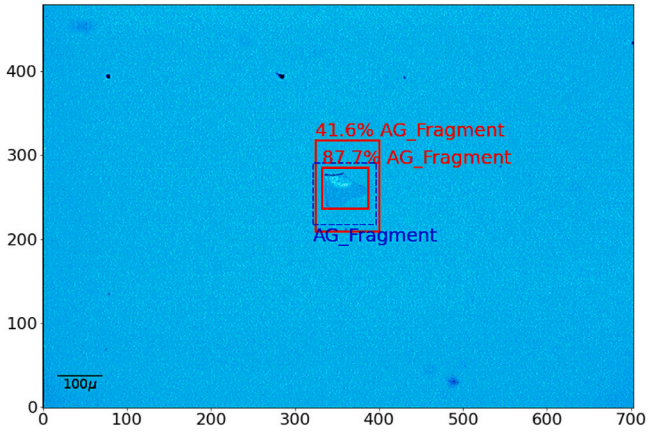


**Fig. 12.** Test data example depicting an aerogel fragment with ground truth bounding box in dashed blue and the network predictions in red. The confidence score of the detected object is also shown at 42% and 88%. Units are pixel coördinates.

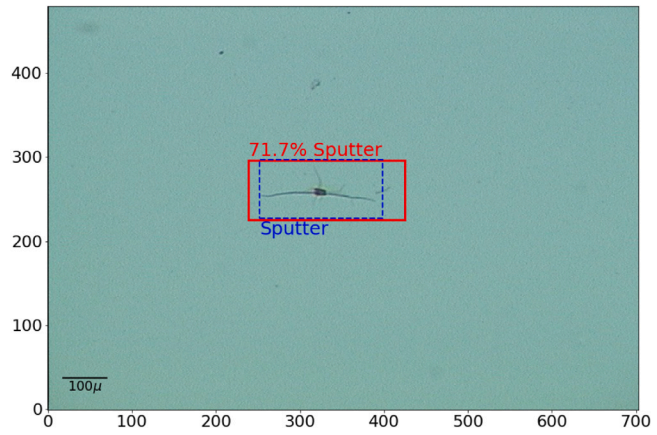


**Fig. 13.** Another output prediction of YOLO-ET applied to test image. The red box shows the predicted bounding box, the annotated classification and confidence probability at 72%. Units are pixel coördinates.

30% confidence level and the overlap of the boxes are less than 50%. Fig. 13 shows another test data example with a single detection. Note the variations in the hues, brightness and contrast of the images that typically make such classifications challenging.

### 4.1. Evaluation metrics

To accurately assess the performance of our network, we utilise a range of evaluation metrics, each chosen for its specific relevance and effectiveness in addressing the unique aspects of our problem. This diverse set of metrics ensures a comprehensive and nuanced understanding of the network's capabilities and weaknesses, allowing for a more targeted and effective optimisation.

#### 4.1.1. Precision and recall

Precision and recall are two fundamental measures used in machine learning for evaluating the performance of classification models, especially in scenarios where the classes are imbalanced. Precision measures the accuracy of the positive predictions made by the model. It is the ratio of true positives (TP, correct detections) to the total predicted positives (both true positives and false positives FP).

$$\text{Precision} = \frac{\text{TP}}{\text{TP} + \text{FP}}. \tag{3}$$

High precision indicates a low false positive rate but does not consider false negatives (FN, missed detections).

Recall measures the ability of the model to find all the relevant cases within a dataset. It is defined as,

$$\text{Recall} = \frac{\text{TP}}{\text{TP} + \text{FN}} \tag{4}$$

High recall indicates that the model is good at finding the positive instances but does not indicate how many negative instances were incorrectly labelled as positive.

The trade-off between precision and recall often depends on the specific requirements of the task. For example with the Tanpopo aerogel-captured surface samples above, if minimising the mis-identification of terrestrial debris particles as extraterrestrial in origin were paramount, then a high precision would help avoid us making incorrect categorisations. On the other hand high recall is essential when the goal is to ensure no potential extraterrestrial particle is missed. This might be prioritised in space environment studies where noting every possible particle is more critical than the occasional false identification. The priority, for Tanpopo surface samples, much like in ML applications for cell pathology, is not to miss anything.

**Table 1**
Confusion matrix based on the test data set.

| | | Predicted | |
|---|---|---|---|
| | | Positive | Negative |
| Actual | Positive | 71 | 15 |
| | Negative | 17 | N/A |

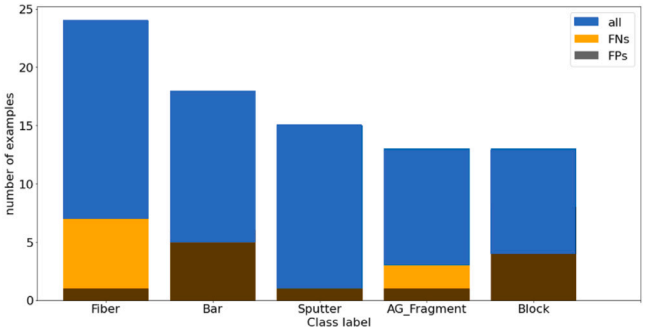


**Fig. 14.** Distribution of FPs and FNs over their classes.

In practice, ML modellers often look at both precision and recall together, sometimes combining them into a single measure called the F1 score, which is the harmonic mean of precision and recall:

$$\text{F1 Score} = \frac{2(\text{Precision} \times \text{Recall})}{\text{Precision} + \text{Recall}} \tag{5}$$

The F1 score provides a balance between precision and recall, considering both false positives and false negatives.

#### 4.1.2. Average precision

We note that the definition of a TP also depends on the IOU threshold with respect to the ground truth box and confidence threshold. Average Precision quantifies the model's performance across different levels of precision and recall, which are typically varied by adjusting the threshold for classifying a detection as a true positive. It is calculated by plotting a Precision–Recall curve, which shows the trade-off between precision and recall for different thresholds. The area under this curve (AUC) represents the AP. Essentially, it is the average of precision values at different recall levels and is specified at a particular IOU threshold.

Mean Average Precision (mAP) is an extension of AP that is used when there are multiple classes to be detected. mAP is the mean of the APs calculated for each class individually. It is computed by first calculating the AP for each class independently. Then these AP values are averaged across all classes. This gives a single metric that summarises the performance across all classes. This is particularly important here where we need to detect multiple types of objects as it gives a holistic view of the model's performance across all these different classes, making it a more comprehensive and balanced metric.

### 4.2. Results

The final loss of our network is 0.8605. YOLO-ET correctly detects 90% of the test data with over 50% overlap (IoU) with the ground truth box. A summary of the results is shown in the confusion matrix (Table 1). Of the False positives, 47% are incorrectly identified as block, 35% as bar and only 1 each of fibre and sputter and aerogel fragment. The FPs are less of a concern as the confidence levels of all the detections are below 50% with the exception of the AG fragment with a confidence of 88%. On inspection this detection is a duplicate detection where 2 bounding boxes are picking up the same object with high confidence. It is also notable that blocks tend to be detected but mis-classified with 3 incorrectly classified as Fib and 2 incorrectly

**Table 2**
Average precision 50 (IOU > 0.5) and mean average precision from the Turi Create environment of the trained YOLO-ET applied to the train and test data from Tanpopo Project aerogel panels. The prioritised classes are grouped morphologically as aerogel fragments, bar, block, fibre and sputter, and likely represent surface residual effects of material released by ISS docking and undocking activities, venting materials, secondary impacts from primary impact ejecta, possible spacecraft component fibres, and fragments of the aerogel itself.

| Class | AG fragment | Bar | Block | Fibre | Sputter | mAP |
|---|---|---|---|---|---|---|
| Train | 0.852 | 0.789 | 0.938 | 0.943 | 0.996 | 0.903 |
| Test | 0.629 | 0.726 | 0.698 | 0.819 | 0.992 | 0.773 |

classified as AG fragment. Fig. 14 shows the distribution of FPs and FNs over their respective class labels. It is evident that the model performs best on detecting and classifying sputter which has the least FNs and FPs. From these values we compute the evaluation metrics, with model attaining a precision, recall and F1 score of 81%, 83% and 82% respectively. Additionally, the Turi Create environment provides tools to easily compute the average precision and mean average precision of the model. These are summarised in Table 2.

These results well surpass the targets set by the Tanpopo Astrobiology Project team of a relatively modest 70% or better recall for surface objects detected on the aerogel panels returned from the ISS, to help ensure that objects of interest and/or entry points to greater depths in the silica aerogel were not being missed. In practice human observers of inanimate objects outperform most convolutional neural networks unless fine-tuned, with overall accuracies of 90% (van Dyck et al., 2021), and YOLO-ET shows performance at these human-comparable levels. At least as notable however is the savings in human labour and computing resource with the implementation of YOLO-ET, and its on-device capabilities for ready real-time use in both laboratory and field environments.

Our F-sample dataset is proprietary to the Tanpopo Project team and currently no other published work exists for comparison, however, in prior work, before the development and implementation of the YOLO-ET system, a VGG-16 network was used but for object classification not detection, and Tanpopo aerogel surface object images at 245x magnification obtained by the CLOXS system were cropped from 704 × 480 pixels to 224 × 224 pixels and used to train a model with highest possible recall.

On the cropped images for most of the surface object categories the project goal of 70% or greater recall was met using the VGG-16 network: 93% for Blocks, 92% for Fibres, and 87% and 83% for Sputter and Bars respectively. Recall performance on Aerogel Fragments was poor however, at 29%. To improve performance a series of image pre-processing tasks were conducted: first a Zero Count Analysis (ZCA) whitening transform (Krizhevsky, 2009; Krizhevsky et al., 2012) was employed to accommodate the different colour hues of the aerogel panels, and next a thresholding sequence, where images were converted to grey scale, noise-reduced, and pixels re-filled against various thresholds, to help create more distinct object boundaries. Both ZCA and thresholding techniques brought Sputter recall to 95%, but there was a somewhat poorer recall performance with thresholding: in the 72%–79% range for Fibres, Blocks and Bars, and still under 70% for Aerogel Fragments, at 62%; ZCA for Aerogel Fragments achieved still only 33% recall.

The low recall rate using the VGG-16 model even with intensive pre-processing, for just one of the five Tanpopo surface object categories necessitated continuing need for human inspection of all panels. The YOLO-ET model and system was thus developed to achieve Tanpopo project recall performance across all categories, without the need for labour-intensive cropping and pre-processing techniques, implemented on a faster network and model that could allow real-time automatic capture on mobile devices. We compare the YOLO-ET model to the performance of VGG-16 on unprocessed data (i.e. no thresholding/ZCA) in Section 4.2 and Section 4.2. Turi Create does not natively

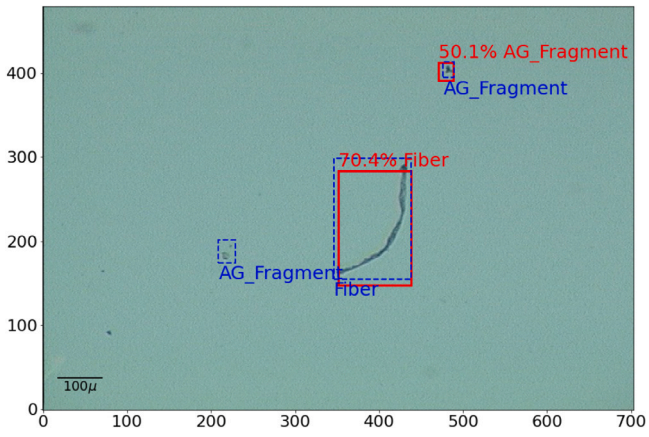


**Fig. 15.** Test image with multiple objects. True labels are shown as dashed blue boxes and model predicted by model CV-3 shown in red with confidence scores.

support K-fold cross-validation (CV) as a built-in feature however, but for purposes of direct comparison with the prior study, we manually created the folds for 4-fold CV and calculate the average Precision and Recall across all folds. In 4-fold CV, the dataset is divided into four equal segments. We then construct and evaluate four distinct models, each trained on a unique combination of three segments for training purposes, thereby ensuring that every segment is utilised once as a testing set. We note that this results in slightly less data available for training the model (75% versus 80%), but the implementation of CV allows us to check for robustness in the model which is important when no validation dataset is available. With no adjustment to Intersection over Union (bounding box overlap thresholds), YOLO-ET trained with this slightly smaller dataset demonstrates comparable if not better performance on Precision but slightly worse on Recall. We note however the models are not directly comparable as the VGG-16 study was an image classification task, where the objects were perfectly centred and cropped down. Our model introduces the additional complexity of object localisation, where images can contain more than 1 object and are not necessarily centred (Fig. 15). The performance accuracy of Image Classification-only models is generally higher than with Object Detection (see e.g. Lin et al. (2018)). But our augmented training dataset is more diverse and furthermore we note that the false negatives in the image classification model VGG-16 are defined as the number of objects incorrectly classified, whereas the false negatives in our model are both the number of objects that are incorrectly classified and those that are not detected. The balance between Precision and Recall is a trade-off, and setting for example a lower confidence threshold and IoU score would typically result in a higher Recall rate whilst reducing Precision. Despite the bigger challenges faced by object detection compared to image classification, by dropping the IoU threshold to 0.3 and the confidence score threshold to 0, the performance of YOLO-ET evaluated on Precision and Recall exceeds that of VGG-16 across all folds (Fig. 16).

Jaeger et al. (2021) also offers useful a useful contrast between Precision and Recall performance in Image Classification versus Object Detection, a study which explores the automatic detection of impact craters on aluminium foils utilising a Convolutional Neural Network (CNN), for Image Classification purposes. Their approach simplifies the problem to binary classification, focusing solely on distinguishing circular craters. Despite this simplification, Jaeger et al. employ synthetic data to train their model. This reliance on synthetically generated craters facilitates their model in achieving an impressive precision rate of 99.8%. However, it is crucial to note that the model's Recall rate stands at 66.7%. This discrepancy between high Precision and relatively lower Recall underscores the challenges inherent in balancing these metrics, particularly when training AI models on synthetic versus authentic datasets.

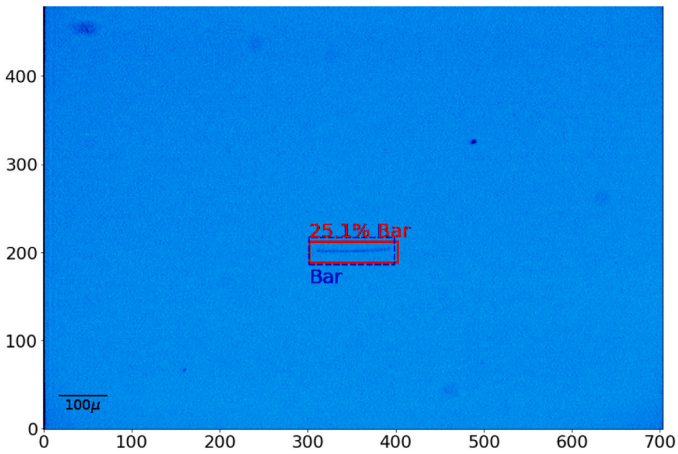


**Fig. 16.** Test image of an object with a low IoU threshold and confidence score of 25.1% that would not typically have made the threshold for positive detection. True labels are shown as dashed blue boxes and model prediction shown in red with confidence score.

| Class | AG frag | Bar | Block | Fibre | Sputter |
|---|---|---|---|---|---|
| VGG-16 | 0.857 | 0.811 | 0.818 | 0.710 | 1.000 |
| CV-0 | 0.929 | 0.938 | 1.000 | 0.944 | 1.000 |
| CV-1 | 0.917 | 1.000 | 0.933 | 0.900 | 1.000 |
| CV-2 | 1.000 | 1.000 | 1.000 | 1.000 | 1.000 |
| CV-3 | 0.824 | 0.857 | 0.963 | 0.947 | 1.000 |
| **CV-avg** | 0.918 | 0.949 | 0.974 | 0.948 | 1.000 |
| CV-std | 0.063 | 0.059 | 0.028 | 0.035 | 0.000 |

Comparison of Precision using a VGG-16 image classification model and our 4-fold cross-validation runs. CV-avg and CV-std are the average and standard deviations of the cross-validation runs.

| Class | AG frag | Bar | Block | Fibre | Sputter |
|---|---|---|---|---|---|
| VGG-16 | 0.286 | 0.833 | 0.931 | 0.917 | 0.872 |
| CV-0 | 0.812 | 1.000 | 1.000 | 0.850 | 1.000 |
| CV-1 | 0.957 | 1.000 | 0.933 | 0.818 | 1.000 |
| CV-2 | 0.875 | 0.500 | 1.000 | 0.833 | 1.000 |
| CV-3 | 0.933 | 1.000 | 0.963 | 1.000 | 0.950 |
| **CV-avg** | 0.894 | 0.875 | 0.974 | 0.875 | 0.988 |
| CV-std | 0.056 | 0.217 | 0.028 | 0.072 | 0.02 |

Comparison of Recall using a VGG-16 image classification model and our 4-fold cross-validation runs. CV-avg and CV-std are the average and standard deviations of the cross-validation runs.

## 5. Deploying the model

Using the methods developed for this project, we have demonstrated that applying AI Machine Learning to 2D aerogel images with YOLO-ET, greatly speeds up and simplifies the identification, localisation, and classification of Tanpopo aerogel-captured surface particles. These advances have been demonstrated to speed the object detection training process, improve accuracy, and consume fewer computing resources, all while taking advantage of the in-built optics and compact form factor of a mobile device. Our model requires no pre-processing of the data. However to truly realise the potential of this model for space missions, it is imperative to address the dependency on traditional microscopy. While the CLOXS system represents significant capabilities in that it can automatically relocate the coordinates of objects of interest and centre the stages accordingly, the YOLO-ET system can now greatly augment these capabilities by identifying, localising and classifying objects on the first pass in real time. The YOLO-ET core Machine Learning models can be readily translated to a mobile device, in this project as an App, allowing the iPhone's camera, enhanced by a LabCam® adaptor, to act as the object detector for untrained, real-world images, with the self-contained iPhone and App able to bound and classify new images based on the core Machine Learning models developed. We propose the integration of this model into a mobile application for both laboratory and space environments, harnessing the capabilities of widely accessible technology like smartphones. This integration marks a significant step toward edge computing, where data processing is performed at or near the source of data generation.

**Table 3**
iPhone Pro Max 12 specs.

| Camera | iPhone Pro Max 12 | |
|---|---|---|
| Ultra Wide | 12 MP | f/2.4 |
| Wide | 12 MP | f/1.6 |
| Telephoto | 12 MP | f/2.2 |

### 5.1. Adapting and integrating LabCam® to CLOXS

Adapting from the most recent developments in field research (e.g. Ateaque, 2022; Meng et al., 2023), we selected the iPhone Pro Max 12 (Table 3) and the LabCam®,[4] a user-friendly combination, for our initial deployment (Fig. 17). The iPhone's advanced camera system, processing power and sophisticated autofocus technology make it an ideal choice for capturing high-quality images of microparticles. This autofocus feature is critical for our application, as it ensures that images are sharp and highly detailed, facilitating accurate Object Detection without the need for manual focus adjustments. Moreover, the convenience, portability and widespread availability of iPhones offer practical advantages for replicating our methodology across diverse settings, particularly fieldwork and applications in resource-constrained environments. While alternatives such as small PCs and specialised AI cameras exist, the iPhone's integrated ecosystem and the availability of sophisticated development tools in Turi Create make it an attractive choice for implementing advanced AI-driven object detection tasks directly on the device.

Meanwhile, the LabCam® attachment enhances the iPhone's capability to function as a makeshift microscope. It is a portable microscope that can be easily taken to the sample, rather than the other way around. This makes it ideal for real-world and real-time *in situ* detection of say micro-particle contaminants on the lunar surface. With the ability to capture images with up to 100x magnification in integration with an iPhone alone, the LabCam® provides an easy to use, ready system for microparticle detection. These capabilities are now being translated to real-time laboratory examination of aerogel panels, to identify, localise

[4] https://www.ilabcam.com/.

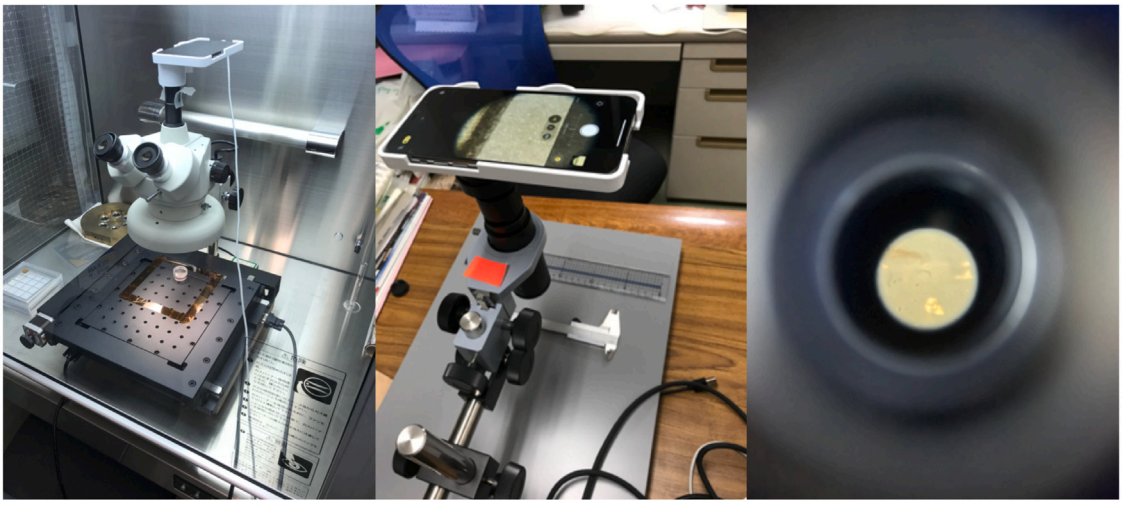

**Fig. 17.** Adapting the LabCam® and iPhone Pro Max 12 into the ISAS CLOXS system. *Left*: Clean bench set up to start single-operator imaging and analysis. Note the LabCam® mount, and 50 mm traverse motorised xy stage, 100 mm traverse stage and joystick controls. *Centre:* Hozon and LabCam® mounted with iPhone Pro Max 12 for calibration. *Right:* Looking remotely 'down the hole' of the iPhone Pro Max 12 at a magnified block particle fragment in the aerogel.

and classify 3D tracks and hypervelocity impact particles candidates, using mobile on-device Machine Learning models.

The combination of the iPhone Pro Max 12, LabCam® mount and integrated magnification, coupled to the CLOXS system at ISAS allows real-time processing to a GPU-equipped desktop running our YOLO-ET algorithms and core Machine Learning model – a full surrogate of what could be packed and space-hardened into *in situ* and in-spaceflight missions. With additional optics added to the system with LabCam®, the CoreML models developed and experiments described in this study demonstrate both real-world laboratory identification and classification of extraterrestrial microparticles and autonomous edge-computing capabilities for future spacecraft missions to detect, localise and classify them.

Thus a unique advantage of the methods employed in this study is that the YOLO-ET imaging and Machine Learning processing and classification is self-contained, with 'on-board' GPU processing whose form factor and computing power can be readily incorporated into small spacecraft. With these applications in mind, further experiments were conducted on identifying and classifying granulated microscopic spacecraft materials distributed atop lunar regolith simulants, as a surrogate for *in situ* detection of anthropogenic contaminants on the lunar surface. Finally, based on the newly returned 'ground truth' of Scanning Electron Microprobe (SEM) images obtained from the asteroid Ryugu sample returned by Hayabusa2, as a further demonstration the model was trained and tested to establish potential correlations with SEM images from the suite of micrometeorites obtained from the TransAntarctic Mountains.

## 6. Discussion

### 6.1. Experiments with spacecraft microparticles on lunar simulants

An anticipated future use of the CLOXS imaging system as adapted and coupled with YOLO-ET in this work is examination of Tanpopo-like aerogel panels deployed and retrieved from the lunar surface. We are developing a mission concept for aerogel panel deployment to the Moon as early as the Artemis lunar landing missions, with important opportunities to advance not only the core Tanpopo astrobiology objectives, but to collect more information and contribute to studies on microparticle anthropogenic contaminants, lunar regolith disturbances by human activities on the Moon, the flux of interplanetary, $\beta$-meteoroids, possible interstellar dust, and secondary impact ejecta (see e.g. Grün et al., 2011; Pokornỳ et al., 2019; Szalay et al., 2020; Costello et al., 2021).

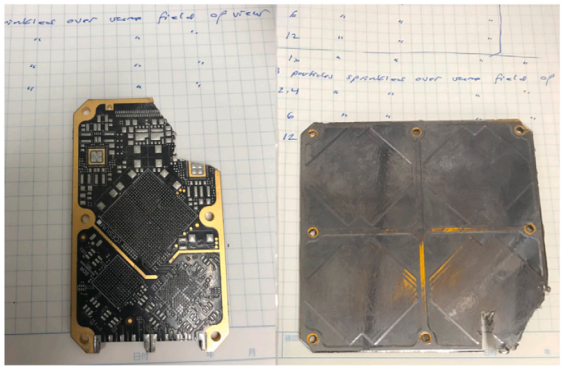

**Fig. 18.** *Left:* SDR board, Polyimide Arlon 85 with SAC 305 solder and copper layers, with impregnation material. *Right:* Nightingale Antenna board, Rogers material with copper and silver coating and STAMET radome.

Ultimately a 'Mini-CLOXS' could support both post-retrieval examination of aerogel panels returned from the lunar surface and other missions to Earth laboratories, as well as *in situ* examination on lunar and other planetary surfaces. A timely factor in bringing these capabilities to the Moon is to help establish a baseline for forward contamination caused by robotic and human activities there. A key element of potential forward contamination are particles of spacecraft, experimental packages, communications equipment etc. that may be deposited and distributed around the Moon by (i) routine operations, including outgassing of propellants and spacesuits, mechanical interfaces, vehicle track and wheel movements, etc.; (ii) natural material degradations from micrometeoroid bombardment, day/night temperature cycles, interaction with the solar wind etc. and (iii) larger scale de-orbited and hard-landed material.

With these in mind we aim to take the YOLO-ET algorithm developed and trained on surface particles captured on the Tanpopo aerogels, and used the same Turi Create, iPhone, and LabCam® system described above to test its capabilities for imaging and identifying spacecraft remnants mixed into lunar regolith simulants.

Samples of both JSC-1 (Appendix A) and Manna Electric lunar simulant (Appendix B) of 0.05 g each were prepared and evenly deposited into 2 cm diameter plastic vials. Test model portions of the CesiumAstro Nightingale satellite (Fig. 18) whose compositions are detailed in (Appendix C) were particulated with a band saw, producing

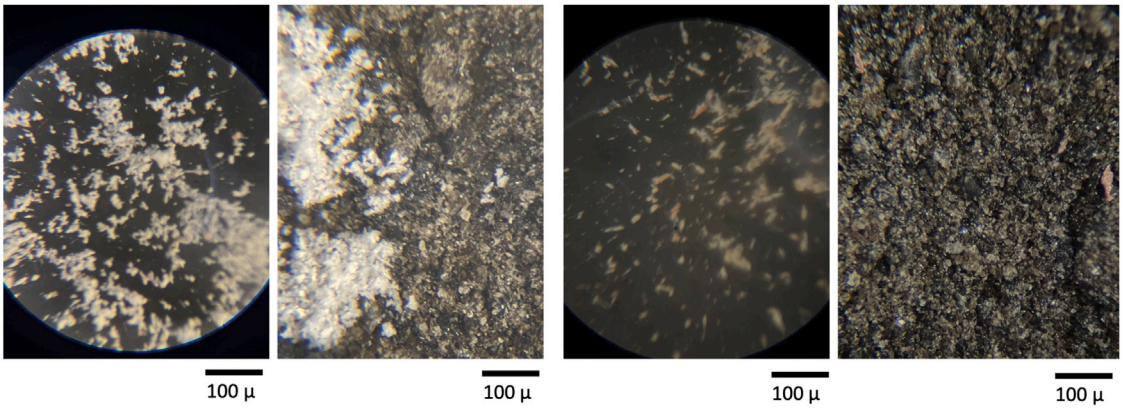


**Fig. 19.** Samples of JSC-1 (Appendix A) lunar simulant of 0.05 g each were prepared and evenly deposited into 2 cm diameter plastic vials. Test model portions of the CesiumAstro Nightingale satellite (Fig. 18) whose compositions are detailed in (Appendix C) were particulated with a band saw, producing spiralled fragments that were then sieved to 80 µm to approximate average JSC-1 grain sizes, to set the challenge to distinguishing similar sized fragments amongst similar sized grains. From left to right: CesiumAstro 'A' particles from the antenna board; A particles on JSC-1; 'B' particles from the Software Defined Radio board; B particles on JSC-1.

spiralled fragments that were then sieved to 80 µm to approximate average JSC-1 grain sizes, to set the challenge to distinguishing similar sized fragments amongst similar sized grains (Fig. 19). YOLO-ET first trained on a limited data set of images of 80 µm diameter glass beads, and then spacecraft grade Al, Ti, and CFRP in various lighting conditions and magnifications, set atop the lunar simulant deposits. Utilising the specially combined optics of a 4x Hozon lab microscope, a 10xLabCam®, and an iPhone Pro Max 12 with 1x-12x magnification, the overall range is 40x to 480x. Optimal experimental resolution for early training and ground truth experiments in YOLO-ET are 100x; with next-generation LabCam® and iPhone Pro Max 15, 225x magnification can be anticipated using purely analogue optics, highly suitable for spacecraft deployment.

At the optimum magnification of 100x, lighting conditions and depth, for which an *in situ* Mini-CLOXS would be designed, early YOLO-ET training and ground truth experiments have been demonstrated to show ready identification of Nightingale antenna particles and Software Defined Radio board microcircuitry particles (Fig. 20), and once optimised the resulting model can be directly exported to CoreML format, for streamlining integration into the on-device application.

### 6.2. Asteroid Ryugu sample experiments

As described above, the YOLO-ET convolutional network models developed and trained on aerogel-captured anthropogenic contaminant samples of the Tanpopo missions onboard the International Space Station using a mobile device camera and new processing techniques greatly speeds and automates their identification and classification. This technique moves beyond datasets that have already been laboriously centred, focused, scaled, photographed, and classed by human researchers, opening the door to automated transits by microscope across the Tanpopo aerogel panels at approximately 500 × 500 pixel increments, at different focal lengths, with images then fed directly into YOLO-ET — which then uses its object detection/localisation capabilities to automatically draw bounding boxes around the object or objects of interest in each image, and to automatically run a confidence prediction of which class of object it might be, displayed both on the image and as a searchable table.

Several of the authors have participated in analyses of samples of the asteroid Ryugu returned by the Hayabusa2 mission (Yada et al., 2022), and the potential for important time-and-manpower gains with YOLO-ET seems clear. Hundreds of nano-CT scans were conducted to create segmented images whose cross-sections helped reveal micro-scale voids of particular interest. Human-eye examination of void evidence in cross-section allowed re-integration of the images to reveal the voids in full dimension. This manual process of identifying and classifying evidence of voids in cross-section is ripe for ML identification, classification, and reintegration using the methods developed in this project. Data from the Ryugu sample A0180 can now form a robust training data set for applying YOLO-ET to other more porous and aggregate samples from Ryugu. With time, the 3D optical images, nano-CT data, and external and internal SEM images from A0180 and other Ryugu samples can be archived to create further training data for searching the diversity amongst different groups of Ryugu samples and for practically comparing characteristic Ryugu micro-structures with for example structures from unmelted micrometeorites, which to the human eye seem to show strikingly similar characteristics and features (Fig. 21).

Accordingly as a demonstration of these abilities YOLO-ET was also trained on SEM images of the Ryugu asteroid sample A0180, to establish 'ground truth' for characterising features of unmelted micrometeorites and unmelted portions of partially melted micrometeorites, using images of the TransAntarctic Mountains micrometeorite suite (Fig. 22). Unlike larger falls, micrometeorites are subject to less heating and alteration as they pass through Earth's atmosphere, and preserve important elements of their formation history and composition. By comparing them for the first time to the ancient base line features of the indigenous asteroidal and cometary samples returned by spacecraft such as Stardust, Hayabusa, Hayabusa2 and OSIRIS-REx, it is possible to re-calibrate current assumptions about e.g. the proportional representation of CI chondrites amongst terrestrial meteorite collections. Many of the characteristic features of each are notably subtle, and typically require considerable training and experience for research practitioners to deduce. In this work YOLO-ET demonstrates capabilities for learning and establishing correlations amongst unseen micrometeoritic data sets.

Distinguishable structural elements amongst images of micrometeorites with unmelted areas include: roughness and irregularities versus the smoother, glassy appearance of melted portions; differences in brightness reflecting compositional differences in backscattered electron images; micro-chondrules, mineral grains and inclusions indicative of parent body origins, otherwise obliterated in melted regions; and distinctive boundaries between melted and unmelted areas, with partial rims characteristically forming around unmelted areas. Based on these types of parameters we trialled, as a proof of concept, making selections of areas of interest on the Ryugu A0180 images, using them to train and predict on a selection of the suite of TransAntarctic Mountain unmelted micrometeorites. Our YOLO-ET model, trained on a limited dataset of 212 examples (without optimisation), detects features in unseen test data. While this showcases the model's potential, the current mean average precision (mAP) is only 10.1%, indicating significant room for improvement.

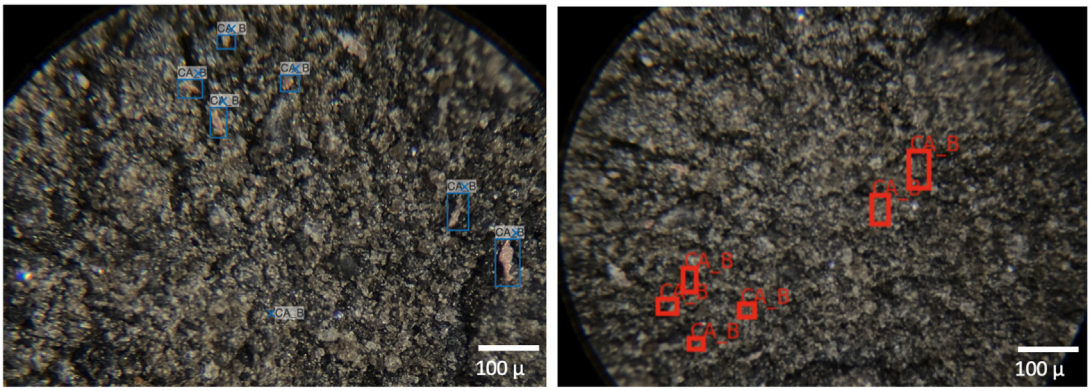


**Fig. 20.** Early applications of our machine learning model YOLO-ET demonstrated that they could be trained on known 'B' particles of CesiumAstro Nightingale Software Defined Radio Board to automatically identify unseen 'B' particles atop JSC-1 Lunar simulant.

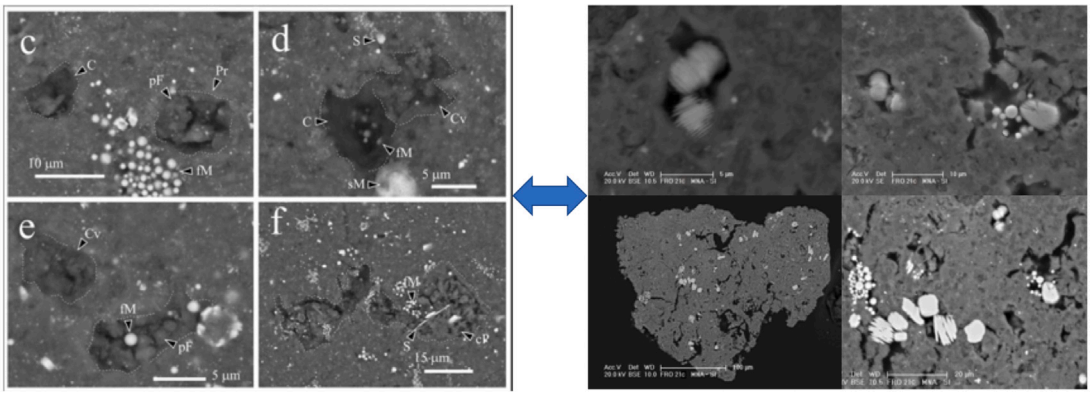


**Fig. 21.** Exploring potential correlations in major features of indigenous asteroid samples Ryugu A0180, left, with those of unmelted micrometeorite samples from the TransAntarctic Mountain micrometeorites suite.
*Image Credits:* Genge et al. (2023) and Van Ginneken et al. (2012).

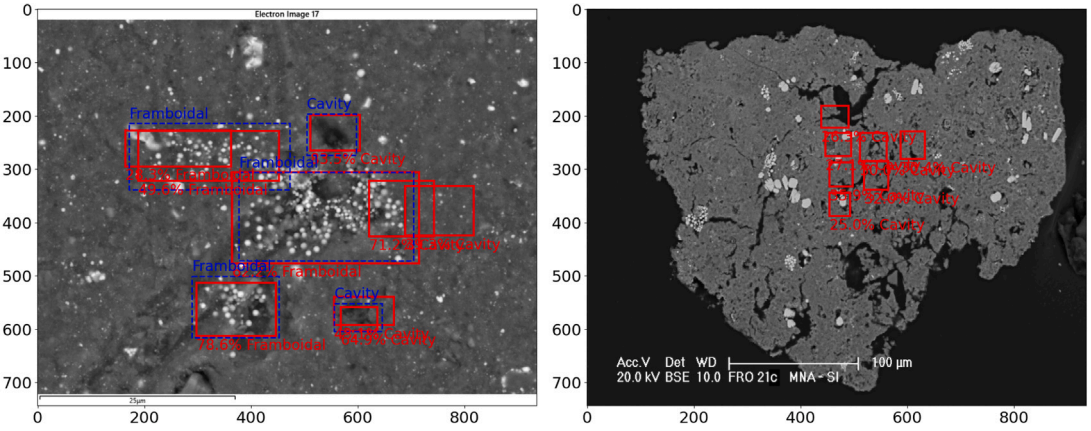


**Fig. 22.** Early applications of our machine learning model YOLO-ET show that training on a Ryugu sample automatically identifies similar features on unmelted TransAntarctic micrometeorites.
*Image Credits:* Genge et al. (2023) and Van Ginneken et al. (2012).

### 6.3. Future work

Future space missions are expected to yield a much larger and more heterogeneous quantity of microscopic materials than treated in these experiments. These include new asteroid interceptions, planetary expeditions, and most especially, robotic and human sample return missions to the Moon, facilitated by unprecedented cargo return capacities. With the imminent rise of robotic and human activities on the Moon, the importance of *in situ* microscopic examination capabilities to distinguish these microparticles becomes increasingly important for (i) identifying and quantifying the flux of anthropogenic contaminants and lunar surface disturbances and (ii) for controlled experiments to better understand the flux of exogenous (IDPs, $\beta$-meteoroids, possible interstellar dust) and indigenous (secondary impact ejecta) microparticles, with important implications for characterising the quantity of volatiles

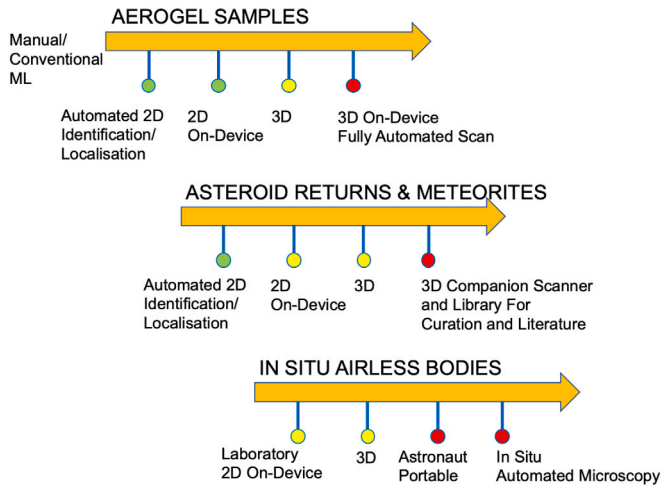


**Fig. 23.** Current and future work: Progressing YOLO-ET on mobile devices from Earth receiving laboratories to *in situ* analyses on airless bodies.

**Fig. 24.** Ispace lunar lander rendering. Startups like ispace are contracting for payloads that could accommodate a mini-CLOXS.
*Credit:* Ispace.

held in micro-structures and their resource potential (see e.g. He et al., 2023) for micro-structure potential.

In addition, researchers may also wish to investigate the possible panspermia delivery of pre-biotic and biotic materials within our Solar System (Napier, 2004). In the longer term, there is also the remoter possibility of discovering trace artefacts of other technological civilisations from across the Galaxy, pushed by radiation pressure and stellar winds (Arkhipov, 1996; Crawford, 2006). If such artefacts exist, they are most likely to be revealed at the microscopic level, upon the mass examination of many trillions of particles uncovered at the scale of industrialised lunar and asteroid mining.

By moving from more conventional Machine Learning approaches to the YOLO-ET model specifically developed here for the detection, localisation and classification of microparticles from and in the space environment, this work has opened the door to rely more on compressed Machine Learning models, existing high-performance GPU code, and commercially available software libraries; we are developing, training and testing algorithms on systems and hardware that would readily fit into a cubesat class spacecraft, lunar rover, or planetary sampling missions (Fig. 23).

For future work inspecting silica aerogels for captured microparticles, we are progressing to fully automated scans in real time in the receiving laboratory clean room environment, and from 2D surface scans to 3D inspection of hypervelocity impact candidates. Similarly, the work on 2D slice SEM images of the Ryugu samples correlated to images of micrometeorites and other asteroid return samples is planned to be extended to 3D images. Moving from Ryugu to Bennu samples may be a natural next step (Goldwin, 2023).

This on-device, mini-CLOXS capability can then be made fully portable and ruggedised to perform scans *in situ* on airless bodies, obviating the need, risks, time and costs for sample return to Earth and better complementing Earth-based studies (Fig. 24).

These capabilities can also be extended from direct observation of micrometeorite particles on Earth to direct observation of microparticles on other planetary surfaces, without aerogel panel capture. Similarly moving from 2D to 3D scans, these devices can serve as companions for Earth-based space microparticle curators and assist in a more complete and integrated cataloguing from both newly collected samples and the extended prior literature. Ultimately, we aim to help create an astronaut-portable, 3D real-time scanning capability for microparticle detection, localisation and classification to assist automated microscopy on the Moon and other airless bodies.

Many of the particles of interest that might be distinguished on the surface of the Moon and other airless bodies, whether from cislunar space operations, asteroid and comet fragment intersections, or possible interstellar dust, may arrive at hypervelocity impact speeds. Thus in future work we plan to have materials similar to those used in the YOLO-ET experiments distinguishing microparticles on lunar regolith simulants, fired at hyper-velocities into monocrystalline target materials, to better scale and model characteristic microcrater morphologies as well as their patterns of vaporisation and spallation. It is envisaged that these tools and techniques can practically be packaged for use on board future mineral assay and mining devices deployed on the Moon and asteroids, to help identify micrometeoroids and other microscopic particles of interest in the surface regoliths.

Finally when contemplating spacecraft-borne YOLO-ET mobile device systems extended to both fly-bys and orbital missions it could be useful to adapt the image detection, localisation and classification processes from the microscopic-particle to the macro scale. Real-time detection of features of interest on the Moon and asteroids to assist selection and navigation of surface sample operations, or to monitor and catalogue spacecraft debris and artefacts, could be amongst the next useful implementations. Thus the scope of future work also includes YOLO-ET analyses of Lunar Reconnaissance Orbiter images for detection and classification of spacecraft hardware on the Moon (Haase et al., 2012; Lesnikowski et al., 2020).

## 7. Conclusions

In this work, we have adapted Turi Create's Object Detection capabilities to identify and classify features in images of extraterrestrial microparticle impacts, microstructures, and anthropogenic debris.

1. Training on images from Tanpopo aerogel panels returned from Japan's Kibo module of the International Space Station, YOLO-ET demonstrates a 90% detection rate for all types of anthropogenic contaminants on aerogel surfaces and shows promising early results for detection of both microparticle contaminants on the Moon and for evaluating asteroid return samples.
2. YOLO-ET significantly improves on earlier ML processes in time savings, performance, and more efficient use of computing resources, and thereby can bring value to Tanpopo CLOXS machine processing by requiring fewer resources to more quickly and accurately identify samples of interest within the aerogel panels for extraction, while reducing contamination risk by more accurately and precisely selecting only those samples of interest, and allowing for the timeliest distribution of extracted samples to analysis groups around the world.
3. Preliminary tests of YOLO-ET's application to identifying spacecraft-derived microparticles in lunar regolith simulant samples and SEM images of Ryugu asteroid samples indicate strong model performance and transfer learning capabilities for future extraterrestrial applications.

Our research provides insights into the practical challenges and solutions associated with applying AI in planetary science, especially in environments where data characteristics differ markedly from those used to train general-purpose Image Classification models. We detail our methodology for dataset preparation, model training, and validation, offering a blueprint for other scientists looking to apply AI in specialised research areas. Our hope is that this work will inspire further research that leverages the power of AI to tackle domain-specific challenges.

## CRediT authorship contribution statement

**L.J. Pinault:** Writing – review & editing, Writing – original draft, Visualization, Validation, Supervision, Software, Resources, Project administration, Methodology, Investigation, Funding acquisition, Formal analysis, Data curation, Conceptualization. **H. Yano:** Writing – review & editing, Writing – original draft, Visualization, Validation, Resources, Methodology, Investigation, Formal analysis, Data curation, Conceptualization. **K. Okudaira:** Resources, Methodology, Formal analysis, Data curation. **I.A. Crawford:** Writing – review & editing, Supervision, Conceptualization.

## Declaration of competing interest

The authors declare the following financial interests/personal relationships which may be considered as potential competing interests: Lewis Pinault reports financial support was provided by Airbus Ventures. If there are other authors, they declare that they have no known competing financial interests or personal relationships that could have appeared to influence the work reported in this paper.

## Data availability

The data that support the findings of this study are available on request from the corresponding author, l.pinault@ucl.ac.uk. The data are not publicly available as Tanpopo Astrobiology Project and Ryugu sample analyses are currently ongoing. The source code for TuriCreate is open source and developers can access, modify and contribute to its development on GitHub at http://github.com/apple/turicreate. Additionally our trained model can be found at https://github.com/LewisJPinault/YOLO-ET.

## Acknowledgements

We thank the anonymous Reviewers for contributing to the improvement of our paper.

Airbus Ventures and Airbus Japan supported LJP and coordinated collaborations with HY at JAXA/ISAS.

Key thanks to Professors Yamagishi, H. Mita, and Dr. J. Imani for all their support to HY's work on the Tanpopo aerogel capture experiments and CLOXS development and operation.

Special thanks to Honaka Kiryu for her work supporting KO in the first applications of CLOXS images using VGG-16 models to tackle the Machine Learning approaches to Tanpopo 'F' sample classification: the images and results obtained were key to evaluating YOLO-ET performance.

CesiumAstro kindly provided test model materials from their Nightingale phased array radar unit.

Manna Electric of Luxembourg kindly provided samples of their lunar regolith simulant, used in their lunar *in situ* resource utilisation process preparations, including for their prospective manufacturing of solar panels on the Moon.

HY and LJP have been working with Matt Genge of Imperial College London, Natasha Almeida of the Natural History Museum in London, Matthias van Ginneken and Penny Wozniakiewicz at the University of Kent Canterbury, and Luigi Folco of Università di Pisa on the asteroid Ryugu A0180 samples returned by Hayabusa2. Their careful sample preparations imaging and analyses have greatly stimulated our thinking on present and future directions for YOLO-ET, and we thank them for their permission to use the images in this paper. The A0180 sample has been loaned to the proposal PI (HY) of this research consortium since 2022, by the JAXA/ISAS Astromaterial Science Research Group through the first international Ryugu sample AO. The authors are most grateful to the Hayabusa2 project team for having successfully returned the indigenous samples from Ryugu to the Earth in 2020.

We thank iDu Optics® (New York, NY, USA) for providing LabCam® adaptors aiding the capture of the images through the iPhones used in this project.

## Appendix A. JSC-1 Lunar simulant components

JSC-1 Specifications https://ares.jsc.nasa.gov/projects/simulants/jsc-1-1a.html

## Appendix B. Components analyses maana electric Mare and highlands Lunar simulants

Lunar Mare Simulant Specifications https://maanaelectric.com/space_solutions/simulant_mare/Lunar Highland Simulant Specifications https://maanaelectric.com/space_solutions/simulant_highland/

## Appendix C. CesiumAstro spacecraft materials ground and sieved to 80 μm

- SDR-1001 – the credit card-sized board with black solder mask
  - CesisumAstro's Gen1 Software-Defined Radio (SDR) product for LEO and airborne applications with 100 MHz IBW, operating from 300 MHz to 6 GHz
  - The board construction:
    - 16-layer PCB constructed of Arlon 85N (polyimide) and copper layers
    - Prepreg layers are 85N with 106, 1080, and 2313 glass weaves
    - Plating is ENIG (gold over electroless nickel)
    - Solder mask is Taiyo PSR-4000 MP Black
  - Solder applied to pads is SAC305
- SAPA-1 – the board with four patches covered in reflective film
  - S-band Antenna Patch Array for LEO applications operating in the 2.45 GHz region
  - The board construction:
    - 6-layer PCB constructed of Rogers 4350B and copper layers
    - Prepreg layers are RO4450F
    - Plating is ENIG (gold over electroless nickel; latest revision of the antenna is in ImAg immersion silver finish)
    - Solder mask is Taiyo PSR-4000 MP
  - The thin film radome on the front face of the antenna is Stamet-sputtered Kapton (Dunmore MO20295)

## References

Arkhipov, A.V., 1996. Extraterrestrial artefacts. Observatory 116, 175–176.

Ateaque, S., 2022. Neurotrophin-3 Signalling in Neurons Derived from Human Embryonic Stem Cells (Ph.D. thesis). Cardiff University.

Chen, L., Li, S., Bai, Q., Yang, J., Jiang, S., Miao, Y., 2021. Review of image classification algorithms based on convolutional neural networks. Remote Sens. 13 (22), 4712.

Costello, E.S., Ghent, R.R., Lucey, P.G., 2021. Secondary impact burial and excavation gardening on the moon and the depth to ice in permanent shadow. J. Geophys. Res.: Planets 126 (9), e2021JE006933.
Crawford, I.A., 2006. The astrobiological case for renewed robotic and human exploration of the moon. Int. J. Astrobiol. 5, 191–197.
Dartois, E., Engrand, C., Brunetto, R., Duprat, J., Pino, T., Quirico, E., Remusat, L., Bardin, N., Briani, G., Mostefaoui, S., et al., 2013. UltraCarbonaceous antarctic micrometeorites, probing the solar system beyond the nitrogen snow-line. Icarus 224 (1), 243–252.
Fei-Fei, L., Deng, J., Li, K., 2009. ImageNet: Constructing a large-scale image database. J. Vis. 9 (8), 1037–1037.
Flynn, G.J., 1994. Interplanetary dust particles collected from the stratosphere: physical, chemical, and mineralogical properties and implications for their sources. Planet. Space Sci. 42 (12), 1151–1161.
Genge, M.J., Almeida, N., Van Ginneken, M., Pinault, L.J., Wozniakiewicz, P., Yano, H., 2023. Ice and liquid water in asteroid Ryugu – Constraints from sample A0180. In: The 14th Symposium on Polar Science, National Institute of Polar Research, November 14-17, 2023 Tachikawa, Tokyo, Japan. pp. 1–2.
Genge, M.J., Van Ginneken, M., Suttle, M.D., 2020. Micrometeorites: Insights into the flux, sources and atmospheric entry of extraterrestrial dust at earth. Planet. Space Sci. 187, 104900.
Girshick, R., 2015. Fast R-CNN. In: Proceedings of the IEEE International Conference on Computer Vision. pp. 1440–1448.
Goldwin, T., 2023. The importance of asteroid sample return. Nat. Geosci. 16, 833.
Goodfellow, I., Bengio, Y., Courville, A., 2016. Deep Learning. MIT Press.
Grishin, K., Mei, S., Ilic, S., 2023. YOLO-CL: Galaxy cluster detection in the SDSS with deep machine learning. doi:10.48550/arXiv.2301.09657, arXiv preprint arXiv:2301.09657.
Grün, E., Horanyi, M., Sternovsky, Z., 2011. The lunar dust environment. Planet. Space Sci. 59 (14), 1672–1680.
Haase, I., Oberst, J., Scholten, F., Wählisch, M., Glser, P., Karachevtseva, I., Robinson, M., 2012. Mapping the apollo 17 landing site area based on lunar reconnaissance orbiter camera images and apollo surface photography. J. Geophys. Res.: Planets 117.
He, H., Ji, J., Zhang, Y., 2023. A solar wind-derived water reservoir on the moon hosted by impact glass beads. Nat. Geosci. 16, 294–300.
Huertas-Company, M., Lanusse, F., 2022. The DAWES review 10: The impact of deep learning for the analysis of galaxy surveys. doi:10.48550/arXiv.2210.01813, arXiv preprint arXiv:2210.01813.
Jaeger, L., Butterworth, A.L., Gainsforth, Z., Lettieri, R., Zevin, D., Ardizzone, A., Capraro, M., Burchell, M., Wozniakiewicz, P., Ogliore, R.C., et al., 2021. Automatic detection of impact craters on al foils from the stardust interstellar dust collector using convolutional neural networks. Meteorit. Planet. Sci. 56 (10), 1890–1904.
Jeffrey, N., Lanusse, F., Lahav, O., Starck, J.-L., 2020. Deep learning dark matter map reconstructions from DES SV weak lensing data. Mon. Not. R. Astron. Soc. 492 (4), 5023–5029.
Jiang, P., Ergu, D., Liu, F., Cai, Y., Ma, B., 2022. A review of YOLO algorithm developments. Procedia Comput. Sci. 199, 1066–1073.
Kawaguchi, Y., Yokobori, S.-I., Hashimoto, H., Yano, H., Tabata, M., Kawai, H., Yamagishi, A., 2016. Investigation of the interplanetary transfer of microbes in the Tanpopo mission at the exposed facility of the international space station. Astrobiology 16 (5), 363–376.
Krizhevsky, A., 2009. Learning Multiple Layers of Features from Tiny Images (Master's thesis). University of Toronto, Master's thesis. University of Toronto.
Krizhevsky, A., Sutskever, I., Hinton, G.E., 2012. Imagenet classification with deep convolutional neural networks. Adv. Neural Inf. Process. Syst. 25.
Kurat, G., Koeberl, C., Presper, T., Brandstätter, F., Maurette, M., 1994. Petrology and geochemistry of antarctic micrometeorites. Geochim. Cosmochim. Acta 58, 3879–3904,.
Lesnikowski, A., Bickel, V.T., Angerhausen, D., 2020. Unsupervised distribution learning for lunar surface anomaly detection. doi:10.48550/arXiv.2001.04634, arXiv preprint arXiv:2001.04634.
Lin, T.-Y., Goyal, P., Girshick, R., He, K., Dollár, P., 2018. Focal loss for dense object detection. doi:10.48550/arXiv.1708.02002, arXiv:1708.02002v2.
Meng, T., Zheng, J., Chen, M., Zhao, Y., Sudarjat, H., MR, A.A., Kulkarni, V., Oh, Y., Xia, S., Ding, Z., et al., 2023. Six-month effective treatment of corneal graft rejection. Sci. Adv. 9 (12), eadf4608.
Mitchell, T.M., 1997. Machine Learning. McGraw Hill.
Nakamura, T., Noguchi, T., Tanaka, M., Zolensky, M.E., Kimura, M., Tsuchiyama, A., Nakato, A., Ogami, T., Ishida, H., Uesugi, M., Yada, T., Shirai, K., Fujimura, A., Okazaki, R., Sandford, S.A., Ishibashi, Y., Abe, M., Okada, T., Ueno, M., Mukai, T., Kawaguchi, J., 2011. Itokawa dust particles: a direct link between S-type asteroids and ordinary chondrites. Science 333 (6046), 1113–1116.
Napier, W., 2004. A mechanism for interstellar panspermia. Mon. Not. R. Astron. Soc. 348, 46–51.
Neubeck, A., Van Gool, L., 2006. Efficient non-maximum suppression. In: 18th International Conference on Pattern Recognition. ICPR'06, Vol. 3, IEEE, pp. 850–855.
Pokornỳ, P., Janches, D., Sarantos, M., Szalay, J.R., Horányi, M., Nesvornỳ, D., Kuchner, M.J., 2019. Meteoroids at the moon: orbital properties, surface vaporization, and impact ejecta production. J. Geophys. Res.: Planets 124 (3), 752–778.
Prasad, M., Rudraswami, N., de Araujo, A., Khedekar, V., 2018. Characterisation, sources and flux of unmelted micrometeorites on earth during the last 50,000 years.. Nat. Sci. Rep. 8887, 1–8.
Redmon, J., Divvala, S., Girshick, R., Farhadi, A., 2016. You Only Look Once: Unified, real-time object detection. In: Proceedings of the IEEE Conference on Computer Vision and Pattern Recognition. pp. 779–788.
Redmon, J., Farhadi, A., 2017. YOLO9000: better, faster, stronger. In: Proceedings of the IEEE Conference on Computer Vision and Pattern Recognition. pp. 7263–7271.
Rojas, J., Duprat, J., Engrand, C., Dartois, E., Delauche, L., Godard, M., Gounelle, M., Carrillo-Sánchez, J., Pokornỳ, P., Plane, J., 2021. The micrometeorite flux at Dome C (Antarctica), monitoring the accretion of extraterrestrial dust on earth. Earth Planet. Sci. Lett. 560, 116794.
Sasaki, S., Imani, J.-Y., Yano, H., 2019. Design, fabrication and evaluation of an aerogel processor CLOXS for the astrobiology mission Tanpopo. Biol. Sci. Space 33, 7–11.
Simonyan, K., Zisserman, A., 2014. Very deep convolutional networks for large-scale image recognition. doi:10.48550/arXiv.1409.1556, arXiv preprint arXiv:1409.1556.
Szalay, J., Pokornỳ, P., Horányi, M., 2020. Hyperbolic meteoroids impacting the moon. Astrophys. J. Lett. 890 (1), L11.
Tabata, M., Kawaguchi, Y., Yokobori, S.-I., Kawai, H., Takahashi, J.-i., Yano, H., Yamagishi, A., 2011. Tanpopo cosmic dust collector: silica aerogel production and bacterial DNA contamination analysis. Biol. Sci. Space 25 (1), 7–12.
Tan, C., Sun, F., Kong, T., Zhang, W., Yang, C., Liu, C., 2018. A survey on deep transfer learning. In: Artificial Neural Networks and Machine Learning–ICANN 2018: 27th International Conference on Artificial Neural Networks, Rhodes, Greece, October 4-7, 2018, Proceedings, Part III 27. Springer, pp. 270–279.
Taylor, A., Baggaley, W., Steel, D., 1996. Discovery of interstellar dust entering the earth's atmosphere. 380. 323-325. 10.1038/380323a0. Nature 380, 323–325.
van Dyck, L.E., Roland, K., Jochen, D.S., Roland, G.W., 2021. Comparing object recognition in humans and deep convolutional neural networks—An eye tracking study. Front. Neurosci. 15.
Van Ginneken, M., Folco, L., Cordier, C., Rochette, P., 2012. Chondritic micrometeorites from the transantarctic mountains. Meteorit. Planet. Sci. 47 (2), 228–247.
Yada, T., Abe, M., Okada, T., et al., 2022. Preliminary analysis of the Hayabusa2 samples returned from C-type asteroid Ryugu. Nat. Astron. 6, 214–220.
Yamagishi, A., Hashimoto, H., Yano, H., Imai, E., Tabata, M., Higashide, M., Okudaira, K., 2021. Four-year operation of Tanpopo: astrobiology exposure and micrometeoroid capture experiments on the JEM exposed facility of the international space station. Astrobiology 21 (12), 1461–1472.
Yamagishi, A., Yokobori, S.-I., Hashimoto, H., Yano, H., Higashide, M., Tabata, M., Imai, E., Yabuta, H., Kobayashi, K., Kawai, H., 2014. Tanpopo: astrobiology exposure and micrometeoroid capture experiments—proposed experiments at the exposure facility of ISS-JEM. Trans. Jpn. Soc. Aeronaut. Space Sci. Aerosp. Technol. Jpn. 12 (ists29), Tk_49–Tk_55.
Yano, H., Fitzgerald, H., Tanner, W., 1994. Chemical analysis of natural particulate impact residues on the long duration exposure facility. Planet. Space Sci. 42, 793–802.
Yano, H., Kibe, S., Deshpande, S.P., Neish, M.J., 1997. The first results of meteoroid and debris impact analyses on the space flyer unit. Adv. Space Res. 20, 1489–1494.
Yano, H., Yamagishi, A., Hashimoto, H., Yokobori, S., Kobayashi, K., Yabuta, H., Mita, H., Tabata, M., Kawai, H., Higashide, M., et al., 2014. Tanpopo experiment for astrobiology exposure and micrometeoroid capture onboard the ISS-JEM exposed facility. In: 45th Annual Lunar and Planetary Science Conference. p. 2934.
Zhou, H., Xiao, Y., Zheng, Z., Yang, B., 2022. YOLOv2-tiny target detection system based on FPGA platform. In: 2022 3rd International Conference on Big Data, Artificial Intelligence and Internet of Things Engineering. ICBAIE, pp. 289–292. doi:10.1109/ICBAIE56435.2022.9985817.